



## Article

# Improving Minutiae Image of Latent Fingerprint Detection on Non-Porous Surface Materials under UV Light Using Sulfur Doped Carbon Quantum Dots from Magnolia Grandiflora Flower

David Nugroho <sup>1</sup>, Won-Chun Oh <sup>2,\*</sup>, Saksit Chanthai <sup>3</sup> and Rachadaporn Benchawattananon <sup>1,\*</sup><sup>1</sup> Department of Integrated Science, Faculty of Science, Khon Kaen University, Khon Kaen 40002, Thailand<sup>2</sup> Department of Advanced Materials Science and Engineering, Hanseo University, Seosan-si 356-706, Korea<sup>3</sup> Materials Chemistry Research Center, Department Chemistry and Center of Excellence for Innovation Chemistry, Faculty of Science, Khon Kaen University, Khon Kaen 40002, Thailand

\* Correspondence: wc\_oh@hanseo.ac.kr (W.-C.O.); rachadaporn@kku.ac.th (R.B.)

**Abstract:** In this study, carbon quantum dots (CQDs) from Magnolia Grandiflora flower as a carbon precursor were obtained using a hydrothermal method under the optimized conditions affected by various heating times (14, 16, 18, and 20 min) and various electric power inputs (900–1400 W). Then, hydrogen sulfide (H<sub>2</sub>S) was added to dope the CQDs under the same manner. The aqueous solution of the S-CQDs were characterized by FTIR, XPS, EDX/SEM, and TEM, with nanoparticle size at around 4 nm. Then, the as-prepared S-CQDs were successfully applied with fine corn starch for detection of minutiae latent fingerprints on non-porous surface materials. It is demonstrated that the minutiae pattern is more clearly seen under commercial UV lamps with a bright blue fluorescence intensity. Therefore, this research has proved that the S-CQDs derived from plant material have a better potential as fluorescent probes for latent fingerprint detection.

**Keywords:** minutiae pattern; carbon dots; latent fingerprint; nanoparticle; forensic science



**Citation:** Nugroho, D.; Oh, W.-C.; Chanthai, S.; Benchawattananon, R. Improving Minutiae Image of Latent Fingerprint Detection on Non-Porous Surface Materials under UV Light Using Sulfur Doped Carbon Quantum Dots from Magnolia Grandiflora Flower. *Nanomaterials* **2022**, *12*, 3277. <https://doi.org/10.3390/nano12193277>

Academic Editors: Constantine D. Stalikas and Antonios Kellarakis

Received: 23 August 2022

Accepted: 19 September 2022

Published: 21 September 2022

**Publisher's Note:** MDPI stays neutral with regard to jurisdictional claims in published maps and institutional affiliations.



**Copyright:** © 2022 by the authors. Licensee MDPI, Basel, Switzerland. This article is an open access article distributed under the terms and conditions of the Creative Commons Attribution (CC BY) license (<https://creativecommons.org/licenses/by/4.0/>).

## 1. Introduction

Fingerprints are considered to be a gold standard for identifying biometrics and scientific evidence in the police field. Fingerprints are unique, and because each person has a different pattern of minutiae, they cannot be changed, unless someone gets into an accident that causes them to not have minutiae latent fingerprint, and they are easy to verify based on the capillary tube-shaped channels at the fingertips, which are connected to the sweat glands [1–8]. Fingerprint detection is currently carried out using some physical or chemical processes to detect the residue of latent fingerprint amino acids, oils, and others. This is because the characteristics of latent fingerprints cannot be seen directly by the naked eye [9–14].

Carbon dots (CQDs) are a member of the nanomaterial family, with the characteristics of a nanometer particle size, biocompatibility, low toxicity, and water-solubility. These CQDs have a photoluminescence characteristic that can be used in several applications, such as bioimaging, as drug carriers, for gene delivery, metal ion detection, sensing, and as nanothermometers. There are two methods for CQDs synthesis. The first is a top-down method by cutting the carbon source material, and it makes use of a bottom-up method involving the carbonization of small molecules. The hydrothermal and microwave method is the second method, which is a bottom-up approach possessing the advantages of energy efficiency, low cost, and convenient operation, and it is mainly used to carbonize organic matter to form luminescence at high temperatures and pressures [15–17]. In this study, we prepared an S-doped-CQDs nanocomposite material synthesized using microwave methods in various conditions to obtain the optimum product.

## 2. Methods and Material

### 2.1. Chemicals and Reagents

Hydrogen sulfide was from Kanto Chemical Co. Inc, Tokyo, Japan. Magnolia Grandiflora flower was collected during a short spring season from our Hanseo University flower park at the Department of Advance Materials Science and Engineering, Haemi-myeon, Seosan-si, Korea.

### 2.2. Synthesis

#### 2.2.1. Preparation of Magnolia Grandiflora Powder

Magnolia Grandiflora flower was cut to small sizes and dried for 48 h at 75 °C in an oven, ground using a laboratory mortar, and then kept at room temperature for further use.

#### 2.2.2. Preparation of S-CQDs with Microwave Method

Here, 5 g of powder was dispersed in 250 mL of DI water, then stirred for 30 min at room temperature. Synthesis was conducted using a commercial microwave at various times (14, 16, 18, and 20 min) and varying wattages (900, 1000, 1100, 1200, 1300, and 1400 W). After obtaining the optimum condition for synthesizing S-CQDs. 5 g of flower powder and 0.05 g of H<sub>2</sub>S added was synthesized in the optimum condition (1400 W and 20 min), and after synthesis, it was centrifuged at 5000 rpm for 10 min and filtered using Whatman paper, and the final product of the S-CQDs (a brown solution) was dried in an oven at 65 °C for 24 h to make powder. Lastly, the final powder of the S-CQDs was stored at room temperature.

#### 2.2.3. Preparation of S-CQDs Detecting Powder

To begin, 0.2 g of S-CQDs and 5 g of commercial starch powder were mixed with 20 mL of DI water. Then, the solution was stirred at RT (room temperature) for 12 h, and then dried at 65 °C for 24 h to make it become powder in an oven. The powder of S-CQDs detection powder was then stored at room temperature.

## 3. Results and Discussion

### 3.1. Fourier-Transform Infrared Spectroscopy (FTIR)

Functional groups from Magnolia Grandiflora were analyzed by FTIR as shown in Figure 1(a), which shows the O-H bond at 3250 cm<sup>-1</sup>. At 2920 cm<sup>-1</sup> a C-H stretching alkene bond was found, ester groups (C=O stretching) were found between 1590 cm<sup>-1</sup>, a N-H bending vibration bond was found at 1510 cm<sup>-1</sup>, ester groups (C=O stretching) were found at 1360 cm<sup>-1</sup>, and the C-O-C bond was found at 1050 cm<sup>-1</sup>. Figure 1(b) shows where the stretching vibration of O=S=O can be seen at 1030 cm<sup>-1</sup>, the O-H stretching bond at 3250 cm<sup>-1</sup>, the alkene bond (C-H stretching) at 2920 cm<sup>-1</sup>, the C=O stretching of ester groups at 1590 cm<sup>-1</sup>, N-H bending vibration bond at 1510 cm<sup>-1</sup>, C=O stretching of ester groups at 1360 cm<sup>-1</sup>, and the C-O-C bond at 1060 cm<sup>-1</sup>. Figure 1(c) shows the results of FTIR analysis from CQDs with corn starch, where it can be seen that the O-H stretching bond appears at about 3280 cm<sup>-1</sup>, the alkane bond of the C-H bond at 2920 cm<sup>-1</sup>, -OH vibration at 1360 cm<sup>-1</sup>, C-O vibration at 1230 cm<sup>-1</sup>, C-O-C stretching bond at 1010 cm<sup>-1</sup>, and that C=C bonding trisubstituted at 850 cm<sup>-1</sup> [18–31].

### 3.2. X-ray Diffraction Analysis (XRD)

X-ray diffraction (XRD) analysis revealed the crystallinity and phase of the material on the synthesized CQDs. Figure 2(a) shows that the diffraction peaks were located at 2θ = 21.38° (002) with an interplanar spacing of 0.415 nm/4.15 Å and peaks at 26.38° (002) with an interplanar spacing of 0.33 nm/3.34 Å, which correspond to the diffraction line of carbon. Figure 2(b) shows that the diffraction peaks were located at 2θ = 21.38° (002) with an interplanar spacing of 0.415 nm/4.15 Å and peaks at 26.38° (002) with an interplanar spacing of 0.33 nm/3.34 Å, which correspond to the diffraction line of carbon, and they show diffraction peaks at 2θ = 40.9° (113) with an interplanar spacing of 0.23 nm/2.28 Å.

After being mixed with starch powder, as shown in Figure 2(c), the crystal structure of S-doped-CQDs shifted due to the combination of carbon dots with flour; the flour had the characteristic of a powder that was lumpier, and its diffraction peaks were located at  $2\theta = 11.67^\circ$  (001),  $18.84^\circ$  (111),  $20.38^\circ$  (020), and  $24.77^\circ$  (211) [32–35].

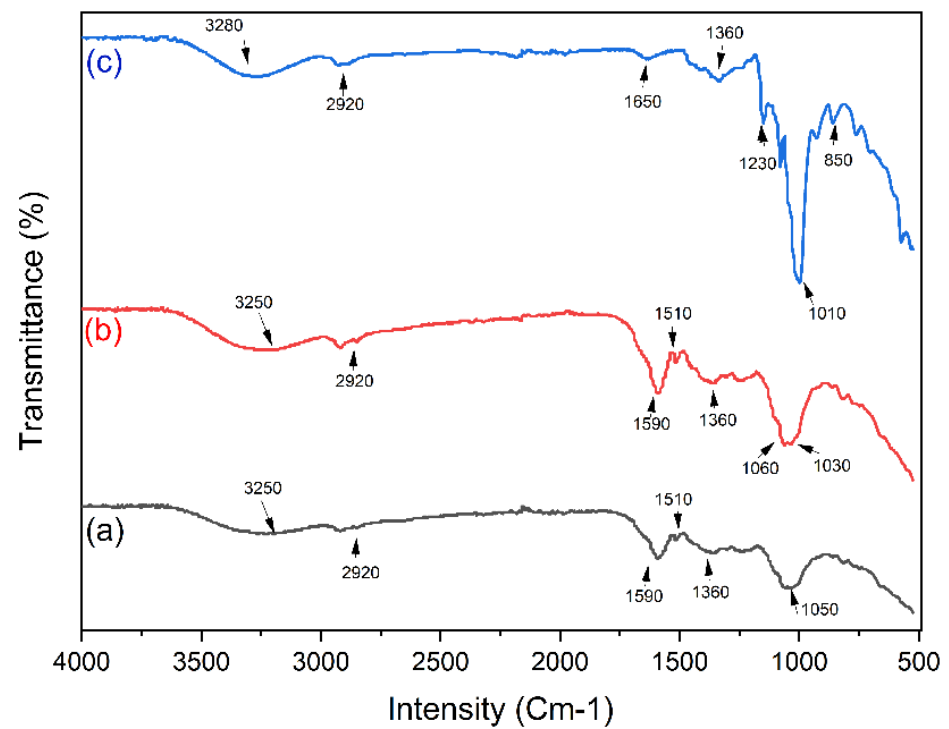


Figure 1. FTIR of (a) CQDs, (b) S-CQDs, and (c) S-CQDs/starch.

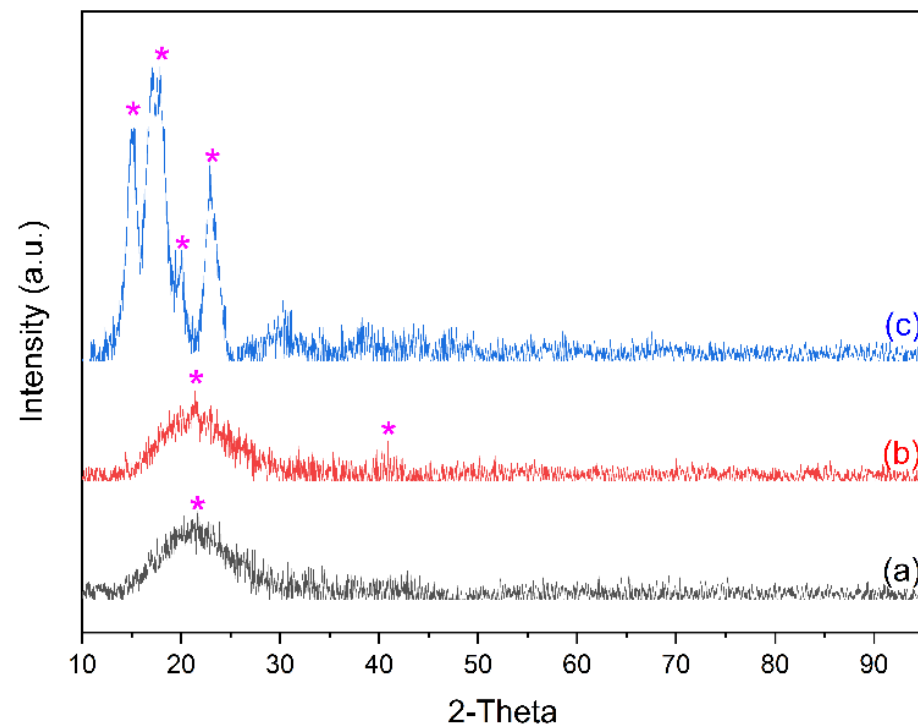
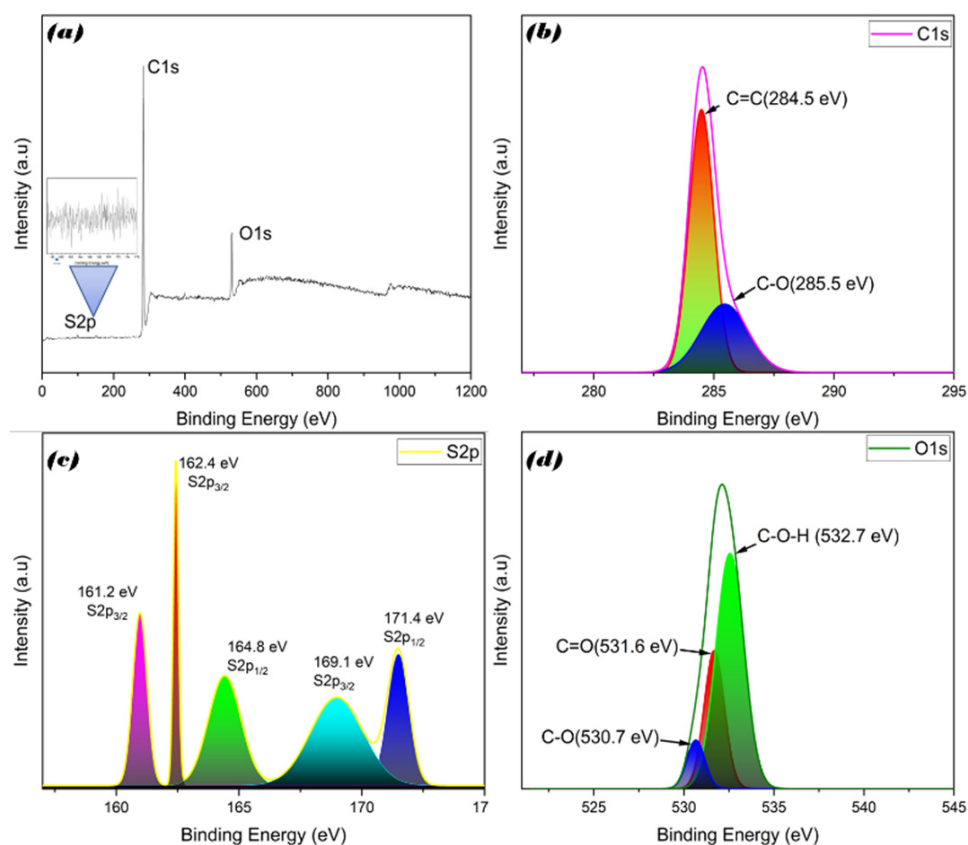


Figure 2. XRD of (a) CQDs, (b) S-CQDs, and (c) S-CQDs/starch.

### 3.3. Elemental X-ray Photoelectron Spectroscopy (XPS) Analysis

The elemental carbon bonding, oxygen bonding, compositions, and sulfur bonding of S-doped-CQDs were analyzed using XPS. The spectrum of the S-doped-CQDs is shown in Figure 3a. Strong peaks at 283.0 and 530.0 eV may, respectively, indicate the energy binding carbon (C 1s) and oxygen (O 1s). The XPS spectra of C 1s (Figure 3b) indicates inadequate carbonization during the heating process by using the microwave method of *Magnolia Grandiflora*, which reveals the presence of C–O and C=C functional groups with deconvoluted binding energies of 284.5 and 285.5 eV, respectively. Substantial numbers of oxygen functional groups were detected in the high-resolution XPS spectra of S-doped-CQDs (Figure 3d) at 531.6, 530.7, and 532.7 eV, which, respectively, corresponded to the C=O, C–O, and C–O–H bonds. The S 2p spectra of S-doped-CQDs (Figure 3c) has two peaks centered at 161.2 and 171.4 eV, indicating that S exists in two forms. The former peak may be deconvoluted into three different components at 161.2, 162.4, and 169 eV, which agree with the  $S2p_{3/2}$ , while the other two peak can be deconvoluted into components at 164.8 and 171.4 eV, which agree with  $S2p_{1/2}$  [36,37].



**Figure 3.** XPS of (a) survey spectrum of S-CQDs, (b) C1s, (c) S2p, and (d) O1s peaks.

### 3.4. Morphological and Optical Property Analysis

Figure 4 shows an image analysis by a TEM, which is consistent with the focused ion FIB-SEM image. The S-doped-CQDs and CQDs has been analyzed for the characterization using TEM, and it is shown in Figure 4e it was found that the particle size of S-doped-CQDs was around 4 nm. Under the FIB-SEM, the surfaces of the CQDs and S-doped-CQDs have been analyzed, and it can be seen in Figure 4a that the surface of CQDs has a smooth texture and a circle shape. Figure 4b shows that, when CQDs mixed with  $H_2S$  become S-doped-CQDs, the texture characteristic changes from smooth to a rough and uneven texture. After the S-doped-CQDs are mixed with starch, it can be seen in Figure 4c that they combine perfectly and make a particle with a sharp texture. The energy-dispersive X-ray

(EDX) of S-doped-CQDs has been analyzed, and it can be seen in Figure 4d that the major elements are C (55.92%) and O (36.57%).

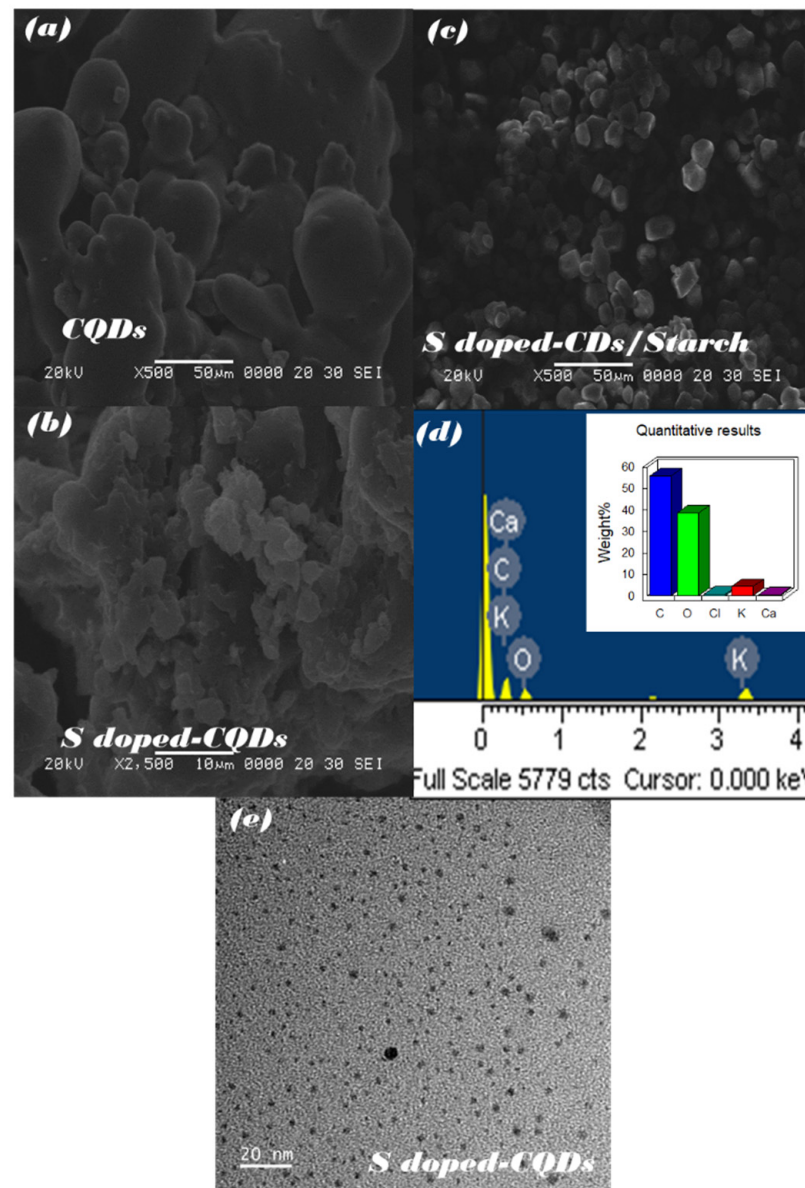


**Figure 4.** FIB-SEM of (a) CQDs, (b) S-CQDs, and (c) S-CQDs/starch; EDX of (d) S-CQDs; TEM of (e)-CQDs.

Optical properties were analyzed in terms of UV–visible absorption and a commercial UV lamp (365 nm). By following Atchudan et al., the CQD was slightly modified by various synthesis durations using microwave methods in varying conditions of time, namely 14, 16, 18, and 20 min, and it was shown that 20 min leads to more blue light under UV lamp, and that 20 min is the optimum condition under UV–Vis spectrophotometer (Figure 5a). The optimum condition for CQDs synthesis has been obtained under microwave by using varying wattage conditions, namely 900, 1000, 1100, 1200, 1300, and 1400 W. Further, under a UV–Vis spectrophotometer, it can be seen that the optimum condition is 1400 W and that there is more blue light under the UV lamp (Figure 5c). After obtaining the optimum conditions, the CQDs were doped with H<sub>2</sub>S to become S-CQDs by adding 0.05 g H<sub>2</sub>S in the optimum condition of the CQDs. The optical properties were monitored, and it was seen that H<sub>2</sub>S can enhance the absorbance from CQDs, and that under UV lamp it also shows more blue light. Figure 5b shows the UV–Vis absorption of CQDs, where it can be

seen that S-CQD displays an absorption peak centered at 270 nm, which is assigned to the  $n \rightarrow \pi^*$  transition of C=O [38] and, for S-CQDs, there is an absorption peak at 310 nm that is assigned to the  $n \rightarrow \pi^*$  transition of C-O [39]. This is similar to previously reported results for carbon quantum dot-based materials, and we can also see that S-CQDs have higher band gap energies than others. After obtaining the optimum condition from the Uv-Vis spectrophotometer analysis, the optimum condition has been checked using a fluorescence spectrophotometer. Figure 5d show the comparison between CQDs and S-CQDs. Here, S-doping from H<sub>2</sub>S has the effect of increasing the intensity of CQDs, with the optimal condition excitation of 370 nm and emission of 455 nm.

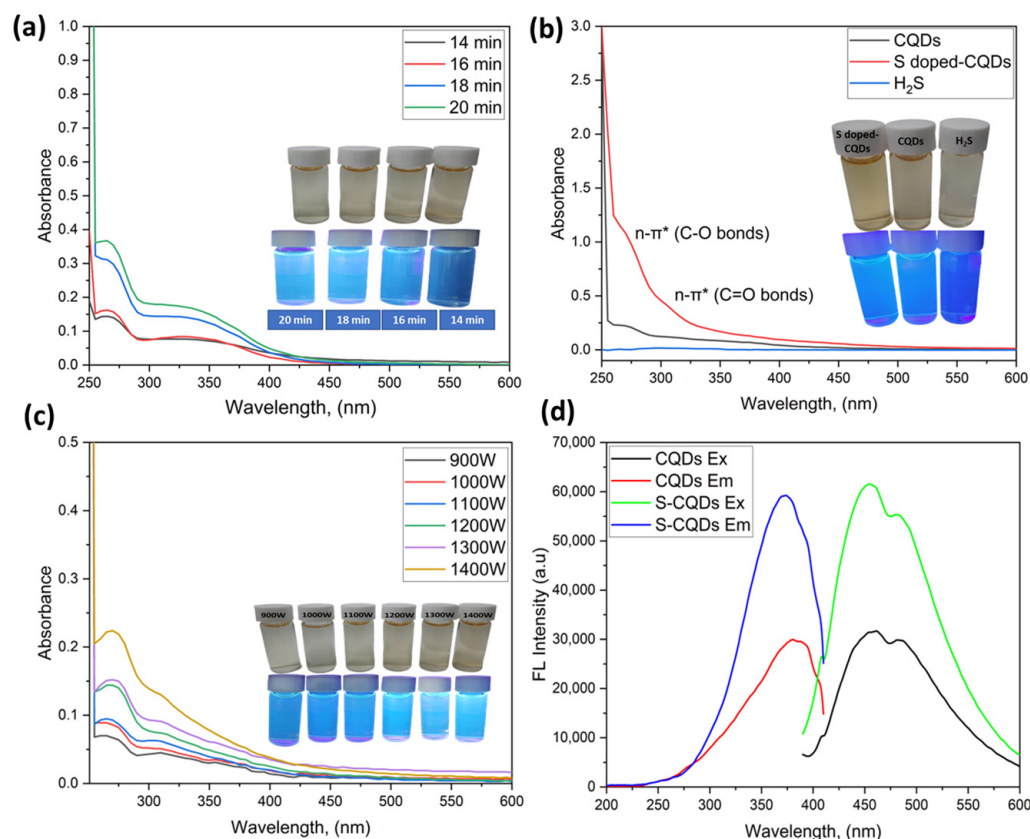


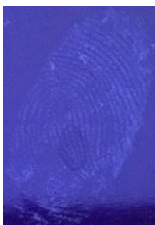
**Figure 5.** Synthesis optimization of S-CQDs: (a) Uv-Vis of the effect of heating time, (b) Uv-Vis of the effect of H<sub>2</sub>S on absorption of CQDs, (c) Uv-Vis of the effect of hydrothermal treatment (W), (d) FL Spectrophotometer of optimum condition (S/W:5/5).

### 3.5. Detection of Latent Fingerprints

#### 3.5.1. Comparison of S-CQDs and CQDs for Latent Fingerprint Detection on Non-Porous Material Surface

The detection of latent fingerprints was tested with the aid of a volunteer who printed his index finger on non-porous material surfaces. Detection powder was brushed on the non-porous surface material, and the latent fingerprint was detected under a normal lamp (LED lamp) and UV lamp (wavelength 365 nm). Latent fingerprint detection was tested on many type of non-porous material surfaces, such as glass, iron, and aluminum foil. Table 1 shows that the detection powder could detect the latent fingerprints on many types of non-porous surface material. Indeed, S-CQDs have a clearer and brighter result under UV lamp, and they can show the minutiae of latent fingerprints compared to the CQDs, but in the normal commercial lamp, neither of them showed it clearly, due to the color of the powder.

**Table 1.** Detection on non-porous surface material using S-CQDs/starch vs. CQDs/starch under normal and UV lamps.

Material Type	CQDs/Starch (Normal Lamp)	CQDs/Starch (UV Lamp)	S-CQDs/Starch (Normal Lamp)	S-CQDs/Starch (UV Lamp)
Knife surface				
Glass surface				
Aluminum surface				

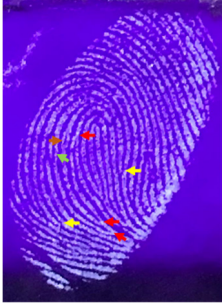
### 3.5.2. Effect of Particle Size Powder for Latent Fingerprint Detection

Capillary lipid protrusions on the tips of the fingers, which contain rows of pores connected to the sweat glands, ensure that everyone has different patterns of fingerprints, and there are very close distances between the lines. In fingerprint detection, particle size dramatically affects the final result from the detection of latent fingerprints [40]. Therefore, in this research, the latent fingerprints have been checked under varying particle sizes. After the S-CQDs detection powder was prepared, the detection powder was sieved using a testing sieve with various pore sizes of 38  $\mu\text{m}$ , 53  $\mu\text{m}$ , and 73  $\mu\text{m}$ . The S-CQD detection powder was brushed onto the material surfaced, and it was detected under a normal lamp and a UV lamp. The result shows that the smallest (38  $\mu\text{m}$ ) particles can show the latent fingerprint minutiae in the most detail (red = bifurcation; yellow = termination; green = island; orange = lake), and this will help criminal investigations (Table 2).

### 3.5.3. Comparison of S-CQDs and Commercial Powder on Latent Fingerprint Detection on Non-Porous Material Surfaces

The detection of latent fingerprints was aided by a volunteer who printed his index finger on non-porous material surfaces. Detection powder was brushed on the fingerprint, which was then detected under a normal lamp (LED lamp) and a UV lamp (wavelength 365 nm). Table 3 shows the comparison of the detection of latent fingerprints on a glass surface material. The S-doped-CQDs have a clearer result under UV lamp; of the total minutiae, nine can be detected, but in the commercial powder it appears clearer under the normal lamp, with a total of eight minutiae detected (red = bifurcation; yellow = termination; green = island; orange = lake).

**Table 2.** Detection of latent fingerprints using different particle sizes of S-CQDs/corn starch under normal and UV lamps.

Particle Size (μm)	S-CQDs/Corn Starch (Normal Lamp)	S-CQDs/Corn Starch (UV Lamp)	Total Minutiae of Latent Fingerprint Can Be Detect
38			Bifurcation: 3 Minutiae Termination: 2 Minutiae Island: 1 Minutiae Orange: 1 Minutiae Total: 7 Minutiae
53			Bifurcation: 2 Minutiae Termination: 1 Minutiae Island: 1 Minutiae Orange: 1 Minutiae Total: 5 Minutiae
73			Bifurcation: 1 Minutiae Termination: 2 Minutiae Island: 1 Minutiae Total: 4 Minutiae

**Table 3.** Detection of latent fingerprints on a glass surface using S-CQDs/starch vs. commercial powder under normal and UV lamps.

Material Type	Commercial Powder (Normal Lamp)	Commercial Powder (UV Lamp)	S-CQDs/Starch (Normal Lamp)	S-CQDs/Starch (UV Lamp)
Glass				

### 3.5.4. Temperature and Storage Time and for Latent Fingerprint Detection

The effects of storage time and temperature for detecting latent fingerprints have also been tested in this research. In this testing, we used a glass material, which had been kept at different temperature conditions ( $-10\text{ }^{\circ}\text{C}$ , Room temp Advanced Materials Science and Engineering Lab, Hanseo University, Korea., and  $60\text{ }^{\circ}\text{C}$ ) at various times. Moreover, the result can be seen in Table 4, which shows that the detection power of S-doped-CQDs can be used to clearly detect the minutiae of latent fingerprints at room temperature until 120 h.

**Table 4.** The effect of storage time and temperature for latent fingerprints detection.

XT	$-10\text{ }^{\circ}\text{C}$	Room Temp. ( $25\text{--}27\text{ }^{\circ}\text{C}$ )	$60\text{ }^{\circ}\text{C}$
24	MD	MD	MD
48	LFD	MD	MD
72	LFD	MD	MD
96	LFD	MD	LFD
120	LFD	MD	LFD

Abbreviations are as follows: MD, minutiae detected; LFD, latent fingerprint detected.

## 4. Conclusions

In this work, we synthesized novel fluorescent S-CQDs via a microwave method by using *Magnolia grandiflora* and hydrogen sulfide as sulfur source. The as-prepared S-CQDs exhibited excellent photostability under various conditions, and the S-CQDs have been characterized under TEM, SEM, XRD, EDX, FTIR, and UV-Vis. Furthermore, S-CQDs are very suitable for the detection of latent fingerprints on non-porous surface materials, and they can also be applied in cases of varying temperatures and varying times of storage. This study provides the detection of latent fingerprint on non-porous material surfaces, and it shows promising results for forensic sciences.

**Author Contributions:** D.N.: validation, analysis, methodology, writing-original draft preparation, and investigation; S.C.: investigation, writing-review and editing; W.-C.O.: conceptualization, investigation, supervision; R.B.: conceptualization, resources and founding research budget. All authors have read and agreed to the published version of the manuscript.

**Funding:** This research was funded by Hanseo University, and Khon Khaen University.

**Institutional Review Board Statement:** Not applicable.

**Informed Consent Statement:** Not applicable.

**Data Availability Statement:** Data can be available upon request from the authors.

**Acknowledgments:** The authors thank financial support to: 1. Department of Advanced Materials Science and Engineering, Hanseo University, Seosan-si 356-706, Korea; 2. Research Center for Environmental and Hazardous Substance Management (EHSM), Khon Kaen University.

**Conflicts of Interest:** The authors declare no conflict of interest.

**Sample Availability:** Samples are available from the authors.

## References

- Prabakaran, E.; Pillay, K. Nanomaterials for latent fingerprint detection: A review. *J. Mater. Res. Technol.* **2021**, *12*, 1856–1885. [[CrossRef](#)]
- Wang, M.; Li, M.; Yu, A.; Zhu, Y.; Yang, M.; Mao, C. Fluorescent Nanomaterials for the Development of Latent Fingerprints in Forensic Sciences. *Adv. Funct. Mater.* **2017**, *27*, 1606243. [[CrossRef](#)] [[PubMed](#)]
- Abdelwahab, W.; Phillips, E.; Patonay, G. Preparation of fluorescently labeled silica nanoparticles using an amino acid-catalyzed seeds regrowth technique: Application to latent fingerprints detection and hemocompatibility studies. *J. Colloid Interface Sci.* **2018**, *512*, 801–811. [[CrossRef](#)]

4. Yuan, C.; Li, M.; Wang, M.; Zhang, X.; Yin, Z.; Song, K.; Zhang, Z. Sensitive development of latent fingerprints using Rhodamine B-diatomaceous earth composites and principle of efficient image enhancement behind their fluorescence characteristics. *Chem. Eng. J.* **2020**, *383*, 123076. [[CrossRef](#)]
5. Li, H.; Guo, X.; Liu, J.; Li, F. A synthesis of fluorescent starch based on carbon nanoparticles for fingerprints detection. *Opt. Mater.* **2016**, *60*, 404–410. [[CrossRef](#)]
6. Milenkovic, I.; Algarra, M.; Alcoholado, C.; Cifuentes, M.; Lázaro-Martínez, J.M.; Rodríguez-Castellón, E.; Mutavdžić, D.; Radotić, K.; Badosz, T.J. Fingerprint imaging using N-doped carbon dots. *Carbon* **2018**, *144*, 791–797. [[CrossRef](#)]
7. Wang, J.; Ma, Q.; Liu, H.; Wang, Y.; Shen, H.; Hu, X.; Tan, W. Time-Gated Imaging of Latent Fingerprints and Specific Visualization of Protein Secretions via Molecular Recognition. *Anal. Chem.* **2017**, *89*, 12764–12770. [[CrossRef](#)]
8. Kumbhakar, P.; Biswas, S.; Pandey, P.; Tiwary, C.; Kumbhakar, P. Tailoring of structural and photoluminescence emissions by Mn and Cu co-doping in 2D nanostructures of ZnS for the visualization of latent fingerprints and generation of white light. *Nanoscale* **2019**, *11*, 2017–2026. [[CrossRef](#)]
9. Xu, C.; Zhou, R.; He, W.; Wu, L.; Wu, P.; Hou, X. Fast Imaging of Eccrine Latent Fingerprints with Nontoxic Mn-Doped ZnS QDs. *Anal. Chem.* **2014**, *86*, 3279–3283. [[CrossRef](#)]
10. Haque, F.; Westland, A.; Milligan, J.; Kerr, M. A small particle (iron oxide) suspension for detection of latent fingerprints on smooth surfaces. *Forensic Sci. Int.* **1989**, *41*, 73–82. [[CrossRef](#)]
11. Bumbrah, G.S. Cyanoacrylate fuming method for detection of latent fingermarks: A review. *Egypt. J. Forensic Sci.* **2017**, *7*, 4. [[CrossRef](#)]
12. Jiao, Y.; Gong, X.; Han, H.; Gao, Y.; Lu, W.; Liu, Y.; Xian, M.; Shuang, S.; Dong, C. Facile synthesis of orange fluorescence 1 carbon dots with excitation independent emission for pH sensing and cellular imaging. *Anal. Chim. Acta* **2018**, *1042*, 125–132. [[CrossRef](#)]
13. Gao, D.; Gao, F.; Kuang, Q.; Zha, X.; Zhang, Z.; Pan, Y.; Jiao, H. Zinc Germanate Nanophosphors with Persistent Luminescence for Multi-Mode Imaging of Latent Fingerprints. *ACS Appl. Nano Mater.* **2022**, *5*, 9929–9939. [[CrossRef](#)]
14. Xu, J.; Zhang, B.; Jia, L.; Fan, Y.; Chen, R.; Zhu, T.; Liu, B. Dual-Mode, Color-Tunable, Lanthanide-Doped Core-Shell Nanoarchitectures for Anti-Counterfeiting Inks and Latent Fingerprint Recognition. *ACS Appl. Mater. Interfaces* **2019**, *11*, 38. [[CrossRef](#)]
15. Koutsogiannis, P.; Thomou, E.; Stamatis, H.; Gournis, D.; Rudolf, P. Advances in fluorescent carbon dots for biomedical applications. *Adv. Phys.-X.* **2020**, *5*, 1758592. [[CrossRef](#)]
16. Zhang, Q.; Zhao, Q.; Fu, M.; Fan, X.; Lu, H.; Wang, H.; Zhang, Y.; Wang, H. Carbon quantum dots encapsulated in super small platinum nanocrystals core-shell architecture/nitrogen doped graphene hybrid nanocomposite for electrochemical biosensing of DNA damage biomarker-8'-hydroxy-2'-deoxyguanosine. *Anal. Chim. Acta* **2018**, *1047*, 9–20. [[CrossRef](#)]
17. Macairan, J.-R.; Jaunky, D.B.; Naccache, R.; Piekny, A. Intracellular ratiometric temperature sensing using fluorescent carbon dots. *Nanoscale Adv.* **2019**, *1*, 105–113. [[CrossRef](#)]
18. Feng, T.; Ai, X.; Ong, H.; Zhao, Y. Dual-Responsive Carbon Dots for Tumor Extracellular Microenvironment Triggered Targeting and Enhanced Anticancer Drug Delivery. *ACS Appl. Mater. Interfaces* **2016**, *8*, 18732–18740. [[CrossRef](#)]
19. Cadd, S.; Islam, M.; Manson, P.; Bleay, S. Fingerprint composition and aging: A literature review. *Sci. Justice* **2015**, *55*, 219–238. [[CrossRef](#)]
20. Benes, H.; Cerna, R.; Durackova, A. Utilization of Natural Oils for Decomposition of Polyurethanes. *J. Polym. Environ.* **2016**, *20*, 175–185. [[CrossRef](#)]
21. Boukir, A.; Fellak, S.; Doumenq, P. Structural characterization of Argania spinosa Moroccan wooden artifacts during natural degradation progress using infrared spectroscopy (ATR-FTIR) and X-Ray diffraction (XRD). *Heliyon* **2019**, *5*, e02477. [[CrossRef](#)] [[PubMed](#)]
22. Djunaidi, M. Gold imprinted adsorption based on eugenol. *J. Phys. Conf. Ser.* **2020**, *1524*, 012077. [[CrossRef](#)]
23. Gopinath, V.; Priyadarshini, S.; Al-Maleki, A.R.; Alagiri, M.; Yahya, R.; Saravanan, S.; Vadivelu, J. In vitro toxicity, apoptosis and antimicrobial effects of phyto-mediated copper oxide nanoparticles. *RSC Adv.* **2016**, *6*, 110986. [[CrossRef](#)]
24. Li, Y.; Kong, D.; Wu, H. Comprehensive chemical analysis of the flower buds of five Lonicera species by ATR-FTIR, HPLC-DAD, and chemometric methods. *Rev. Bras. Farm.* **2018**, *28*, 533–541. [[CrossRef](#)]
25. Razali, N.; Conte, M.; McGregor, J. The role of impurities in the La<sub>2</sub>O<sub>3</sub> catalysed carboxylation of crude glycerol. *Catal. Lett.* **2019**, *149*, 1403–1414. [[CrossRef](#)]
26. Rehman, A.; Eze, V.; Resul, M.; Harvey, A. A kinetic study of Zn halide/TBAB-catalysed fixation of CO<sub>2</sub> with styrene oxide in propylene carbonate. *Green Process. Synth.* **2019**, *8*, 719–729. [[CrossRef](#)]
27. Rozali, M.; Ahmad, Z.; Isa, M. Interaction Between Carboxy Methylcellulose And Salicylic Acid Solid Biopolymer Electrolytes. *Adv. Mater. Res.* **2015**, *1107*, 223–229. [[CrossRef](#)]
28. Sim, L.; Gan, S.; Chan, C.; Yahya, R. ATR-FTIR studies on ion interaction of lithium perchlorate in polyacrylate/poly(ethylene oxide) blends. *SAA* **2010**, *76*, 287–292. [[CrossRef](#)] [[PubMed](#)]
29. Brozek-Pluska, B.; Musial, J.; Kordek, R.; Abramczyk, H. Analysis of Human Colon by Raman Spectroscopy and Imaging-Elucidation of Biochemical Changes in Carcinogenesis. *Int. J. Mol. Sci.* **2019**, *20*, 3398. [[CrossRef](#)]
30. Ilin, A.; Velasco, F.; Navarro, R.; Tornos, F. New data on Alpine type fluorite deposits: Case of Lújar mine in Betic Cordillera (SE Spain). *Macla* **2019**, *24*, 63–64.
31. Travlou, N.; Secor, J.; Badosz, T. Highly luminescent S-doped carbon dots for the selective detection of ammonia. *Carbon* **2019**, *114*, 544–556. [[CrossRef](#)]

32. Varga, G.; Kozma, V.; Kolcsár, V.; Kukovecz, Á.; Kónya, Z.; Sipos, P.; Szollosi, G.  $\beta$ -Isocupreidinate–CaAl-layered double hydroxide composites—heterogenized catalysts for asymmetric Michael addition. *Mol. Catal.* **2020**, *482*, 110675. [[CrossRef](#)]
33. Wang, Y.; Zhou, Q.; Li, B.; Liu, B.; Wu, G.; Ibrahim, M.; Sun, G. Differentiation in MALDI-TOF MS and FTIR spectra between two closely related species *Acidovorax oryzae* and *Acidovorax citrulli*. *BMC Microbiol.* **2012**, *12*, 182. [[CrossRef](#)] [[PubMed](#)]
34. Gupta, B.; Kumar, N.; Panda, K.; Kanan, V.; Joshi, S.; Fisher, I. Role of oxygen functional groups in reduced graphene oxide for lubrication. *Sci. Rep.* **2017**, *7*, 45030. [[CrossRef](#)]
35. Qie, L.; Chen, W.; Xiong, X.; Hu, C.; Zou, F.; Hu, P.; Huang, Y. Sulfur-Doped Carbon with Enlarged Interlayer Distance as a High-Performance Anode Material for Sodium-Ion Batteries. *Adv. Sci.* **2015**, *2*, 1500195. [[CrossRef](#)]
36. Qiu, B.; Cai, L.; Zhang, N.; Tao, X.; Chai, Y. A Ternary Dumbbell Structure with Spatially Separated Catalytic Sites for Photocatalytic Overall Water Splitting. *Adv. Sci.* **2020**, *7*, 1903568. [[CrossRef](#)] [[PubMed](#)]
37. Shanthi, P.; Hanumantha, P.; Ramalinga, K.; Gattu, B.; Datta, M.; Kumta, P. Sulfonic Acid Based Complex Framework Materials (CFM): Nanostructured Polysulfide Immobilization Systems for Rechargeable Lithium–Sulfur Battery. *J. Electrochem. Soc.* **2019**, *166*, A1827–A1835. [[CrossRef](#)]
38. Urana, S.; Alhani, A.; Silva, C. Study of ultraviolet-visible light absorbance of exfoliated graphite forms. *AIP Adv.* **2017**, *7*, 035323. [[CrossRef](#)]
39. Li, S.; Li, Y.; Cao, J.; Zhu, J.; Fan, L.; Li, X. Sulfur-Doped Graphene Quantum Dots as a Novel Fluorescent Probe for Highly Selective and Sensitive Detection of  $\text{Fe}^{3+}$ . *Anal. Chem.* **2014**, *86*, 10201–10207. [[CrossRef](#)]
40. Nugroho, D.; Keawprom, C.; Chanthai, S.; Oh, W.-C.; Benchawattananon, R. Highly Sensitive Fingerprint Detection under UV Light on Non-Porous Surface Using Starch-Powder Based Luminol-Doped Carbon Dots (N-CDs) from Tender Coconut Water as a Green Carbon Source. *Nanomaterials* **2022**, *12*, 400. [[CrossRef](#)]